Plasmonic-Based Imaging of Local Square Wave Voltammetry

ARTICLE *in* ANALYTICAL CHEMISTRY · JULY 2011

Impact Factor: 5.64 · DOI: 10.1021/ac201392r · Source: PubMed

4 AUTHORS, INCLUDING:

Xiaonan Shan
Arizona State University
36 PUBLICATIONS **473** CITATIONS
SEE PROFILE

Shaopeng Wang
Arizona State University
76 PUBLICATIONS **3,177** CITATIONS
SEE PROFILE

Published in final edited form as:
Anal Chem. 2011 October 1; 83(19): 7394–7399. doi:10.1021/ac201392r.

Plasmonic-based Imaging of Local Square Wave Voltammetry

Xiaonan Shan[1,2], **Shaopeng Wang**[1], **Wei Wang**[1], and **Nongjian Tao**[1,2]

[1]Center for Bioelectronics and Biosensors, Biodesign Institute, Arizona State University, Tempe, Arizona 85287, United States

[2]Department of Electrical Engineering, Arizona State University, Tempe, Arizona 85287, United States

Abstract

Square wave voltammetry (SWV) is widely used in electrochemical analysis and sensors because of its high sensitivity and efficient rejection of background current, but SWV by conventional electrochemical detection method does not provide spatial resolution. We report here a plasmonic method to image local SWV, which opens the door for analyzing heterogeneous electrochemical reactions and for high throughput detections of microarrays. We describe the basic principle, validate the principle by comparing the plasmonic-based SWV with those obtained with the conventional method, and demonstrate imaging capability for local electrochemical analysis.

Electrochemical (EC) detection has matured into a powerful analytical tool for various applications, from trace chemical analysis, glucose and neurotransmitters monitoring, to protein and DNA microarray detections. Conventional EC methods measure the total current from an electrode, which does not have spatial resolution to measure local EC reactions. Spatial resolution is needed for studying heterogeneous reactions[1–2], for monitoring single cell activities[3], and for high throughput reading of microarrays[4]. To provide EC methods with spatial resolution, Scanning Electrochemical Microscopy (SECM) has been developed, which maps local EC current by scanning a microelectrode across a sample surface[5–6]. Although SECM has found numerous applications, mechanical scanning of the microelectrode limits its imaging speed and the proximity of the scanning microelectrode to the reaction sites may perturb the reactions. Furthermore, the measured current scales with the electrode area, which leads to a decreasing signal when one attempts to improve the spatial resolution by decreasing the electrode size. Other imaging techniques, including Scanning Tunneling Microscopy, Atomic Force Microscopy and optical interference microscopy[7] have been developed to provide high-resolution structural information of an electrode surface, but they do not measure electrochemical reaction current. SPR has been applied to electrochemical system, while they focused on electric field[8] or potential distribution[9].

We have recently demonstrated a plasmonic-based electrochemical current imaging (PECI) technique that can map local current of an electrode with sub-micron resollution[10]. Instead of probing local EC current point by point electrically with a microelectrode, PECI technique images the local EC current optically by measuring the refractive index change near the electrode surface due to local EC reaction. Because oxidation or reduction of an

Corresponding Author njtao@asu.edu.

ASSOCIATED CONTENT

Supporting Information. Determination of constants, α and β, plasomonic-based SWV of $[Fe(CN)_6]^{3/4-}$ + 0.2 M NaF electrolyte and one video clips demonstrate the PECI video at different potentials. This material is available free of charge via the Internet at http://pubs.acs,org.

analyte is almost always accompanied by a change in the optical property of the analytes, the approach is quite universal. In addition to high spatial resolution, PECI is fast and non-invasive, and its signal does not decrease with the size of a region of interest[10]. We have previously shown that PECI can provide local cyclic voltammetry (CV). Although popular, CV suffers from background current that often places a practical limit on EC detection. Square Wave Voltammetry (SWV) has become a widely used EC detection technique because of its high sensitivity and superior capability to suppress unwanted background current. Important applications of SWV includes DNA damage detection[4, 11], trace chemical analysis[12–13] and protein detections[14]. However, SWV requires fast response time of the detection system, which poses a technical challenge to imaging techniques. Furthermore, capacitive charging needs to be considered when developing PECI of SWV. Here we establish a method to perform local SWV with PECI.

THEORY

EC current includes two major contributions: faradaic current which originates from oxidation or reduction of analyte molecules on the electrode, and non-faradaic current due to, e.g., capacitive charging current. Conventional EC methods measure both faradaic and non-faradaic currents. Likewise, PECI also measures both the faradaic and non-faradaic contributions. The former is measured, as pointed earlier, via EC reaction-induced change in the refractive index of the analytes. In contrast, the latter is measured because plasmonic signal is sensitive to surface charge density of the electrode, which has been used in our recent work[15–16] to image electrochemical interfacial impedance.

We express the total plasmonic signal ($\Delta\theta$) at a given location and time as a sum of faradaic ($\Delta\theta_f$) and non-faradaic ($\Delta\theta_c$) contributions, or

$$\Delta\theta(x,y,t)=\Delta\theta_f(x,y,t)+\Delta\theta_c(x,y,t)=\beta\int_0^t i_f(x,y,t')(t-t')^{-1/2}dt'+\frac{1}{\alpha}\int_0^t i_c(x,y,t)dt \quad (1)$$

$$\beta=B\left(\alpha_R D_R^{-\frac{1}{2}}-\alpha_O D_O^{-\frac{1}{2}}\right)(nF\pi^{1/2})^{-1},$$

$$\alpha=-\frac{ed_m n_e \varepsilon_2(\varepsilon_2+\varepsilon_m)^2\sin(2\theta_R)}{\varepsilon_1^2(\varepsilon_m-1)}.$$

where i_f and i_c are the corresponding faradaic current and charging current, α and β are the constants[15, 17] that can be determined independently (see supporting materials).

In order to measure the electrochemical activity of a target analyte, one needs to suppress unwanted background current in electrochemical analysis. This task is accomplished in conventional SWV by applying a square wave potential superimposed on a linearly sweeping potential to the electrode. The current response to each square wave has two components, faradaic current and charging current. The latter component changes exponentially with time, and reaches a steady state faster than the former. So by measuring current at the end of each square wave, right before the next, the transient charging current is suppressed. In PECI, we apply the same potential waveform to the entire electrode and measure the plasmonic response in each electrode region. From the local plasmonic signal vs. time, we determine local current vs. time, and then obtain local SWV by measuring the current at the end of each square wave. To simplify signal/data processing, we may exclude

the second term when calculating the EC current. As we will show later, including the second term in Eq. 1 leads to only a small baseline shift in the SWV, which is the essence of SWV for minimizing background current.

EXPERIMENTAL SECTION

Experimental Setup

The plasomonic imaging setup is based on the widely used Krechmann configuration (Scheme 1),[18] which comprises a light emitting diode (LED) light source (670 nm), collimating lens, prism, imaging optics, polarizer, and a CCD camera. A microscope cover slide coated with 47 nm thick Au film was coupled optically to the prism surface via index of refraction matching fluid. The plasmonic image was captured at up to 380 frames per second, allowing for measurements of the plasmonic response induced by the applied potential waveform.

Reagents and Solutions

Hexaammine-ruthenium (III) chloride ($[Ru(NH_3)_6]Cl_3$), potassium ferricyanide ($K_3[Fe(CN)_6]$), potassium hexacyanoferrate (II) trihydrate ($K_4[Fe(CN)_6]\cdot 3H_2O$) and sodium fluoride (NaF) were purchased from Sigma Aldrich and were used as received. All aqueous solutions were prepare from PURELAB ultra (>18.2 MΩ cm^{-1}) water.

Square Wave Voltammetry

SWV was performed at room temperature using a Teflon EC cell fixed on top of the Au film, which was also served as the working electrode. Potential waveform with frequency 10 Hz, pulse height 50 or 25 mV and a potential step 10 mV or 5 mV was applied to the Au electrode with an Autolab potentiostat using a Pt wire and Ag/AgCl/KCl as counter electrode and reference electrode, respectively. We studied redox reaction of 10 mM of $Ru(NH_3)_6^{3+}$ or 20 mM of $[Fe(CN)_6]^{3-}$ and $[Fe(CN)_6]^{4-}$ mixture (1:1 ratio) in 0.2 M NaF solution. A Matlab program was used to determine PECI from the plasmonic signals. The setup was capable of simultaneously recording the total electrochemical current with the conventional EC method, and acquiring PECI of the electrode.

Surface Modification

To demonstrate local SWV imaging capability, a patterned hexadecanethiol monolayer was created by soft lithograph technique.[19] 2 mM-hexadecanethiol in ethanol solution was applied to PDMS stamp surface by cotton Q-Tips. After drying the stamp with N2 for 15 s, it was then brought into contact with the Au film for 5–10 s.

RESULTS AND DISCUSSION

PECI of SWV

To validate PECI of SWV, we first carried out SWV measurements on an Au electrode in 10 mM $Ru(NH_3)_6^{3+}$ simultaneously with the plasmonic imaging and conventional electrochemical approaches. Figure 1a shows the potential waveform applied to the electrode, which is composed of square waves superimposed on a linearly sweeping potential from 0 to −0.3 V. The corresponding plasmonic response over an area of 1.8×1.3 mm^2 of the electrode is shown in Figure 1b. The plasmonic response is initially small (0 to ~ 0.5 s), which is almost entirely due to capacitive charging effect because the potential is far more positive than the formal potential of the redox reaction (~ −0.16 V). The response increases and reaches a maximum as the potential sweeps to the formal potential (at ~ 2 s), and then decreases again and returns to the capacitive charging background.

From the plasmonic response vs. time, we determined the current using the algorithm described in Ref. 6, and the result as a function of potential is shown in Figure 1d. For each square wave there is a forward (in the direction of potential sweep) and reverse potential steps. In the present case, the potential sweeps negatively, so the forward potential step is in the negative potential direction. Figure 1d shows that each forward potential step induces a sudden drop in the current, followed by a fast rise and then a slow rise in the current. The fast rise is due to capacitive charging process, and the slow rise is due to electrochemical reaction (faradaic current). Associated with each reverse potential step, the current response is reversed, as expected. The simultaneously recorded current by the conventional method is shown in Figure 1c, which is in quantitative agreement with the plasmonic-based current. Note that the sharp spikes on the first several cycle of conventional method (Figure 1c) does not appear on the PECI method which is caused by data sampling rate. This observation demonstrates that the algorithm to convert plasmonic signals into electrochemical current works well not only for a linearly sweeping potential but also for a potential waveform containing sharp potential steps.

Like the conventional SWV, we extracted the current shown in Figure 1d at the end of each forward potential step, and denote it as forward current, I_f (green triangles, Figure 1e). The forward current vs. potential shows a trough near −0.15 V. Similarly, we obtained the reverse current, I_r, from the end of each reserve potential step, vs. potential (blue stars in Figure 1e), which shows a peak near −0.15 V. The difference between the forward and reverse currents, I_f-I_r, vs. potential is the SWV, shown as red stars in Figure 1e. For comparison, we plotted the corresponding I_f, I_r, and I_f-I_r obtained with the conventional SWV in Figure 1f. It is clear that the plasmonics-based SWV and the conventional SWV are excellent agreement with each other. We also studied $[Fe(CN)_6]^{3/4-}$ in 0.2M NaF using the same approach, and observed quantitative agreement between the SWVs obtained by the plasmonic and conventional approaches (see supporting information).

Charging Effects

To examine how capacitive charging affects the PECI, we performed two plasmonic SWV measurements. The first measurement was carried out in the pure supporting electrolyte, 0.2 M NaF solution, and the result shown as the green curve in Figure 2a is due to background current (e.g., capacitive charging current). The second measurement was in 10 mM $Ru(NH_3)_6^{3+}$ + 0.2 M NaF solution, and the plasmonic response contains contributions from both the redox reaction of $Ru(NH_3)_6^{3+}$ and background current (red curve, Figure 2a). By subtracting the background current in the first measurement from the SWV in the second measurement, we obtained a charging effect-corrected plasmonic response of SWV, shown as the blue curve in Figure 2a (shift up 30 intensity units). Note that after subtraction, the plasmonic response to the square waves near the beginning (0 to −0.05 V) and end (−0.275 to −0.30 V) of the potential sweep drops to nearly zero, indicating effective correction of the capacitive charging contribution.

From the plasmonic responses (Figure 2a), we determined the current with (blue curve in Figure 2b) and without (red curve in Figure 2b) correcting the background current. Zooming-in of two square waves shows that although the capacitive charging associated with each potential step leads to a large transient current in the beginning (Figure 2c), its contribution decreases rapidly over time, and becomes negligible near the end of a potential step. Figure 2d compares SWVs (I_f -I_r vs. potential) with and without background current correction. We can see that the two SWVs are similar except for a small baseline shift. The baseline shift is due to the capacitive charging effect associated with the linearly sweeping potential, which is also present in the conventional SWV.

Local PECIs at Different SWV Potential

In order to demonstrate SWV imaging capability with PECI, we studied heterogeneous electrochemical reactions with a Au surface patterned by hexadecanethiol monolayer. Figure 3a is a conventional surface plasmon resonance image, in which the bright patterns correspond to the hexadecanethiol-covered region, and the dark background is the bare Au surface. We performed SWV imaging of the surface in 20 mM $[Fe(CN)_6]^{3/4-}$ + 0.2 M NaF electrolyte. Figure 3b shows SWVs of three selected regions on the electrode, two from the bare Au area (marked by blue and green squares in Figure 3a) and one from the thiol-covered area (red square in Figure 3a). Each SWV was obtained from the plasmonic signal averaged over the corresponding region. The thiol-covered region shows only a flat baseline, due to effective blockage of the redox reaction by the thiol monolayer. In contrast, the bare Au regions show pronounced peaks near 0.25 V in the SWVs due to the redox reaction of $[Fe(CN)_6]^{3/4-}$. Although both bare Au regions display the redox peak, the peak amplitudes are different, which reflects different amounts of thiol "contamination" during the contact printing in the two regions.

It is also possible to obtain SWV at each pixel of the plasmonic image, which provides a SWV image, from which a SWV from each pixel is obtained. Figures 3c-f show a few snapshots of such SWV images at several different potentials, and a video showing SWV image during potential sweep is provide in the Supporting Materials. At 0 V, the image (Figure 3c) shows only noise, which is expected because no measurable redox reaction takes at the potential. Increasing the potential to +0.18V (closer to the formal potential), the current in the thiol-covered regions remain small but the current in the bare Au region increases substantially, leading to high contrast images of the patterned surface (Figure 3d). When the potential increases to +0.23 V, the thiol-covered region still shows no current while the current in the bare Au regions reaches maximum (Figure 3e). Further increasing the potential, the current in the bare Au regions decreases again (Figure 3f). This spatial information and SWV imaging capability are not available in the conventional SWV.

CONCLUSION

In conclusion, we have developed a plasomonic method to image local SWV. The SWV averaged over an electrode is in quantitative agreement with the simultaneously recorded SWV obtained by the conventional electrochemical method, which validates the plasmonic-based SWV. We have demonstrated SWV imaging capability and applied it to study local electrochemical reactions on a surface. This capability is not possible with the conventional electrochemical methods, and we believe that it is particularly suitable for electroanalysis of heterogeneous reactions and for electrochemical detection of microarrays.

Supplementary Material

Refer to Web version on PubMed Central for supplementary material.

Acknowledgments

We thank NIH (R21RR026235) and NSF (CHE-0554786) for support.

REFERENCES

1. Fernandez JL, Walsh DA, Bard AJ. Thermodynamic guidelines for the design of bimetallic catalysts for oxygen electroreduction and rapid screening by scanning electrochemical microscopy. M-Co (M : Pd, Ag, Au). Journal of the American Chemical Society. 2005; 127:357–365. [PubMed: 15631486]

2. Sanchez-Sanchez CM, Solla-Gullon J, Vidal-Iglesias FJ, Aldaz A, Montiel V, Herrero E. Imaging Structure Sensitive Catalysis on Different Shape-Controlled Platinum Nanoparticles. Journal of the American Chemical Society. 2010; 132 5622-+
3. Mellander L, Cans AS, Ewing AG. Electrochemical Probes for Detection and Analysis of Exocytosis and Vesicles. ChemPhysChem. 2010; 11:2756–2763. [PubMed: 20737529]
4. Fojta M. Electrochemical sensors for DNA interactions and damage. Electroanalysis. 2002; 14:1449–1463.
5. Amemiya S, Bard AJ, Fan F-RF, Mirkin MV, Unwin PR. Scanning Electrochemical Microscopy. Annual Review of Analytical Chemistry. 2008; 1:95–131.
6. Schulte A, Nebel M, Schuhmann W. Scanning Electrochemical Microscopy in Neuroscience. Annual Review of Analytical Chemistry. 2010; 3:299–318.
7. Wen R, Lahiri A, Azhagurajan M, Kobayashi S, Itaya K. A New in Situ Optical Microscope with Single Atomic Layer Resolution for Observation of Electrochemical Dissolution of Au(111). J. Am. Chem. Soc. 2010; 132:13657–13659. [PubMed: 20839798]
8. Hanken DG, Corn RM. Electric field measurements inside self-assembled multilayer films at electrode surfaces by electrochemically modulated surface plasmon resonance experiments. Israel Journal of Chemistry. 1997; 37:165–172.
9. Flatgen G, Krischer K, Pettinger B, Doblhofer K, Junkes H, Ertl G. 2-DIMENSIONAL IMAGING OF POTENTIAL WAVES IN ELECTROCHEMICAL SYSTEMS BY SURFACE-PLASMON MICROSCOPY. Science. 1995; 269:668–671. [PubMed: 17758810]
10. Shan XN, Patel U, Wang SP, Iglesias R, Tao NJ. Imaging Local Electrochemical Current via Surface Plasmon Resonance. Science. 2010; 327:1363–1366. [PubMed: 20223983]
11. Fu LM, Lin CH. High-resolution DNA separation in microcapillary electrophoresis chips utilizing double-L injection techniques. Electrophoresis. 2004; 25:3652–3659. [PubMed: 15565701]
12. Wang J, Thongngamdee S. On-line electrochemical monitoring of (TNT) 2,4,6-trinitrotoluene in natural waters. Analytica Chimica Acta. 2003; 485:139–144.
13. de Sanoit J, Vanhove E, Mailley P, Bergonzo P. Electrochemical diamond sensors for TNT detection in water. Electrochim. Acta. 2009; 54:5688–5693.
14. Naumann R, Schmidt EK, Jonczyk A, Fendler K, Kadenbach B, Liebermann T, Offenhausser A, Knoll W. The peptide-tethered lipid membrane as a biomimetic system to incorporate cytochrome c oxidase in a functionally active form. Biosensors & Bioelectronics. 1999; 14:651–662.
15. Foley KJ, Shan X, Tao NJ. Surface impedance imaging technique. Anal. Chem. 2008; 80:5146–5151. [PubMed: 18484741]
16. Wang W, Foley K, Shan X, Wang SP, Eaton S, Nagaraj VJ, Wiktor P, Patel U, Tao NJ. Single cells and intracellular processes studied by a plasmonic-based electrochemical impedance microscopy. Nature Chemistry. 2011; 3:249–255.
17. Wang SP, Huang XP, Shan XN, Foley KJ, Tao NJ. Electrochemical Surface Plasmon Resonance: Basic Formalism and Experimental Validation. Anal. Chem. 2010; 82:935–941. [PubMed: 20047281]
18. Kretschmann E. Determination of Optical Constants of Metals by Excitation of Surface Plasmons. Zeitschrift Fur Physik. 1971; 241:313–324.
19. Deng T, Wu H, Brittain ST, Whitesides GM. Prototyping of Masks, Masters, and Stamps/Molds for Soft Lithography Using an Office Printer and Photographic Reduction. Anal. Chem. 2000; 72:3176–3180. [PubMed: 10939384]

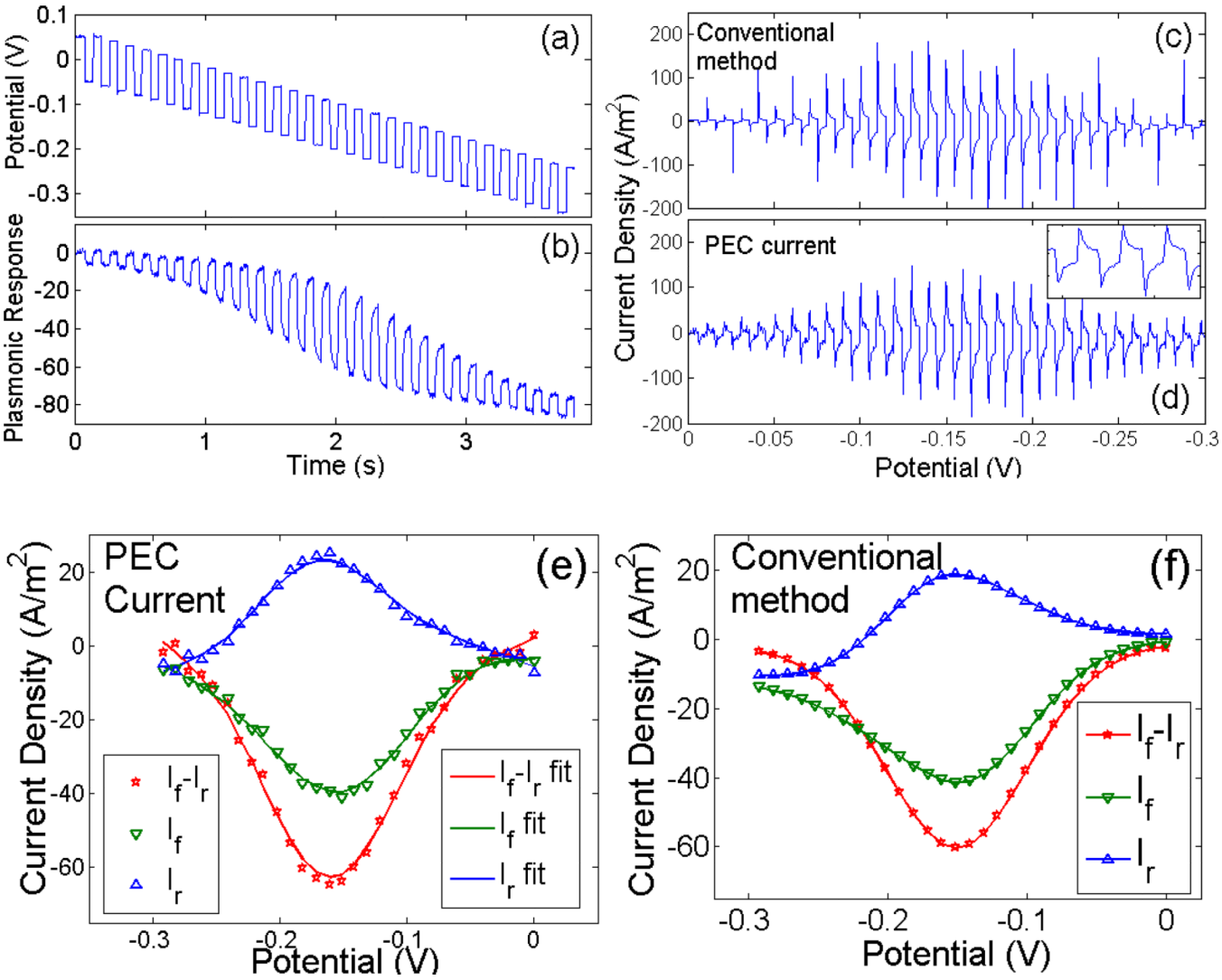

Figure 1.

(a) Potential waveform for SWV. It consists of square waves superimposed on a linear potential, sweeping from 0 to −0.3 V. (b) Plasmonic response due to the potential waveform shown in (a). (c) Transient current density vs. potential obtained with the conventional electrochemical method. (d) Transient current density vs. potential of the same electrode obtained with the plasmonic-based method. (e) SWV obtained with the plasmonic method. (f) SWV obtained with the conventional electrochemical method. I_f and I_r in (e) and (f) are forward current and reverse current, extracted at the end of each of the forward potential step, and reverse potential step, respectively.

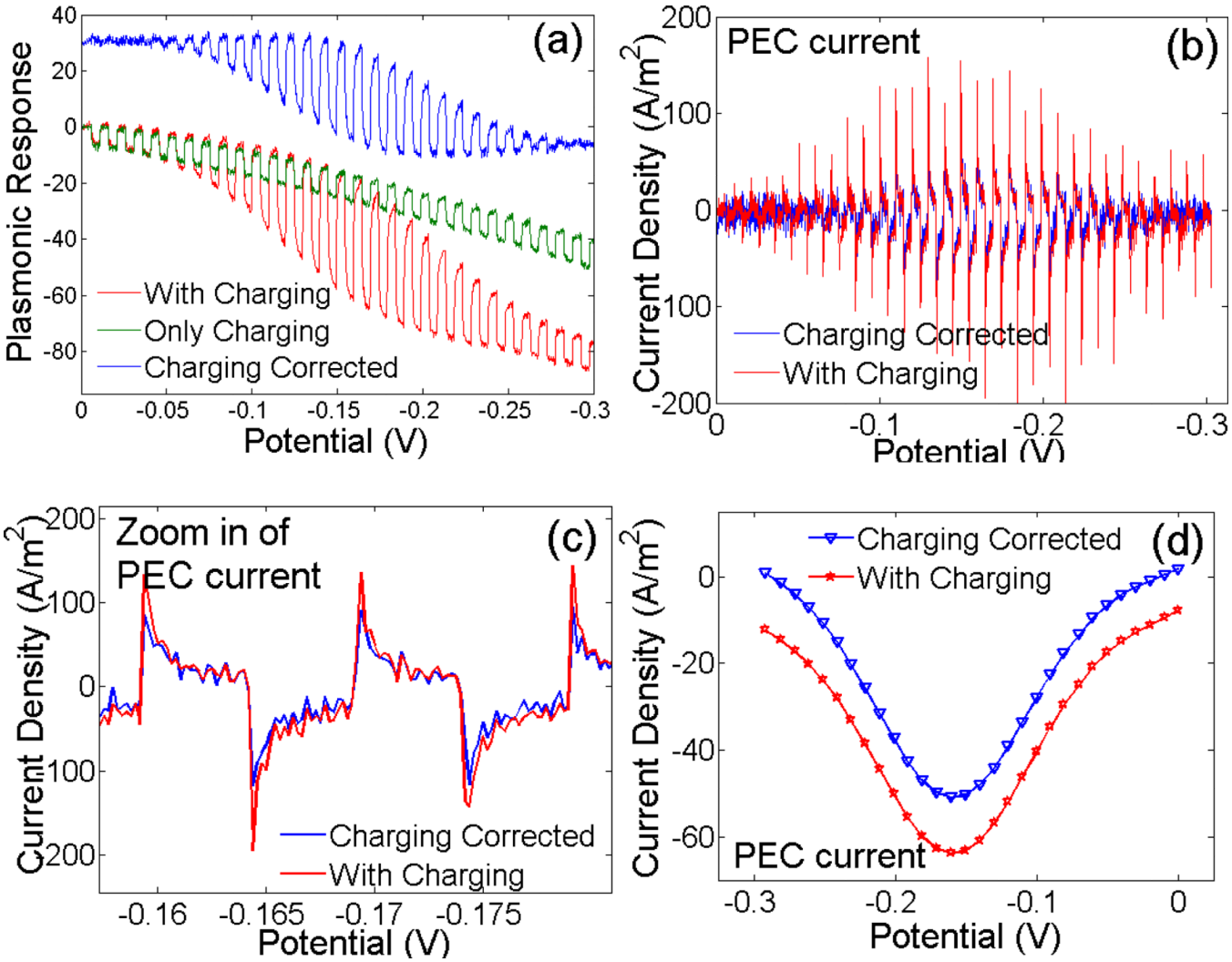

Figure 2.

(a) Plasmonic responses in 10 mM $Ru(NH_3)_6^{3+}$ + 0.2 M NaF (red) and in 0.2 M NaF (green). The former contains both the redox reaction current and background current, while the latter contains only the background current. The difference of the two (blue) taken by subtracting the red curve from the blue curve presents background corrected SWV. Note that for clarity the background corrected SWV is shifted up by 30 units. (b) Corresponding plasmonic current densities vs. potential. (c) Zooming-in of current density signals of two potential steps. (d) SWVs with (red) and without correction of the background charging effect (blue).

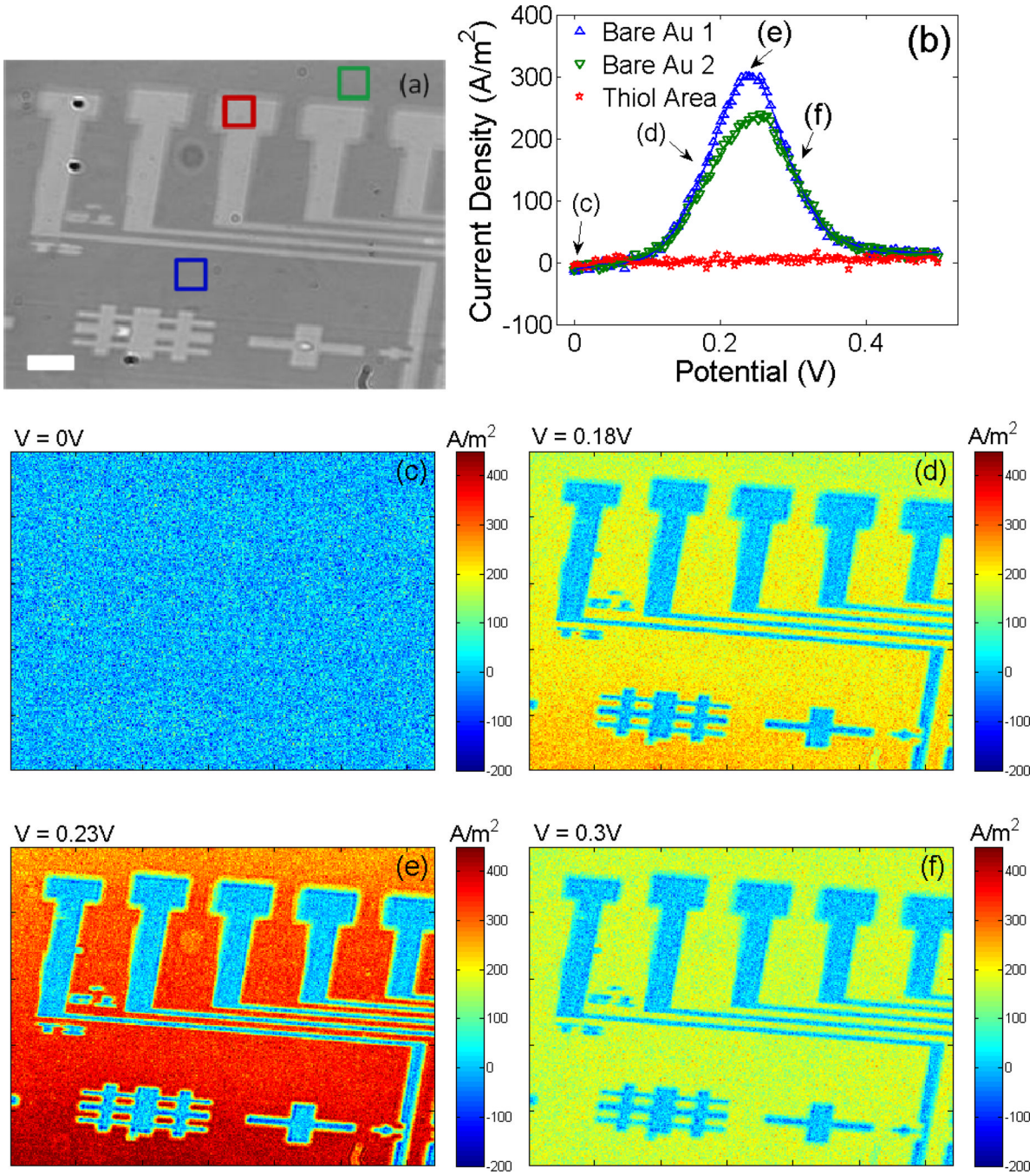

Figure 3.

(a) Surface Plasmon resonance image of a Au surface patterned with thiols (the surface potential was not controlled), the scale bar is 100μm. (b) Local SWVs of the regions marked in (a). (c-f) Snapshots of SWV video of the surface at different potentials (which are pointed out in (b)).

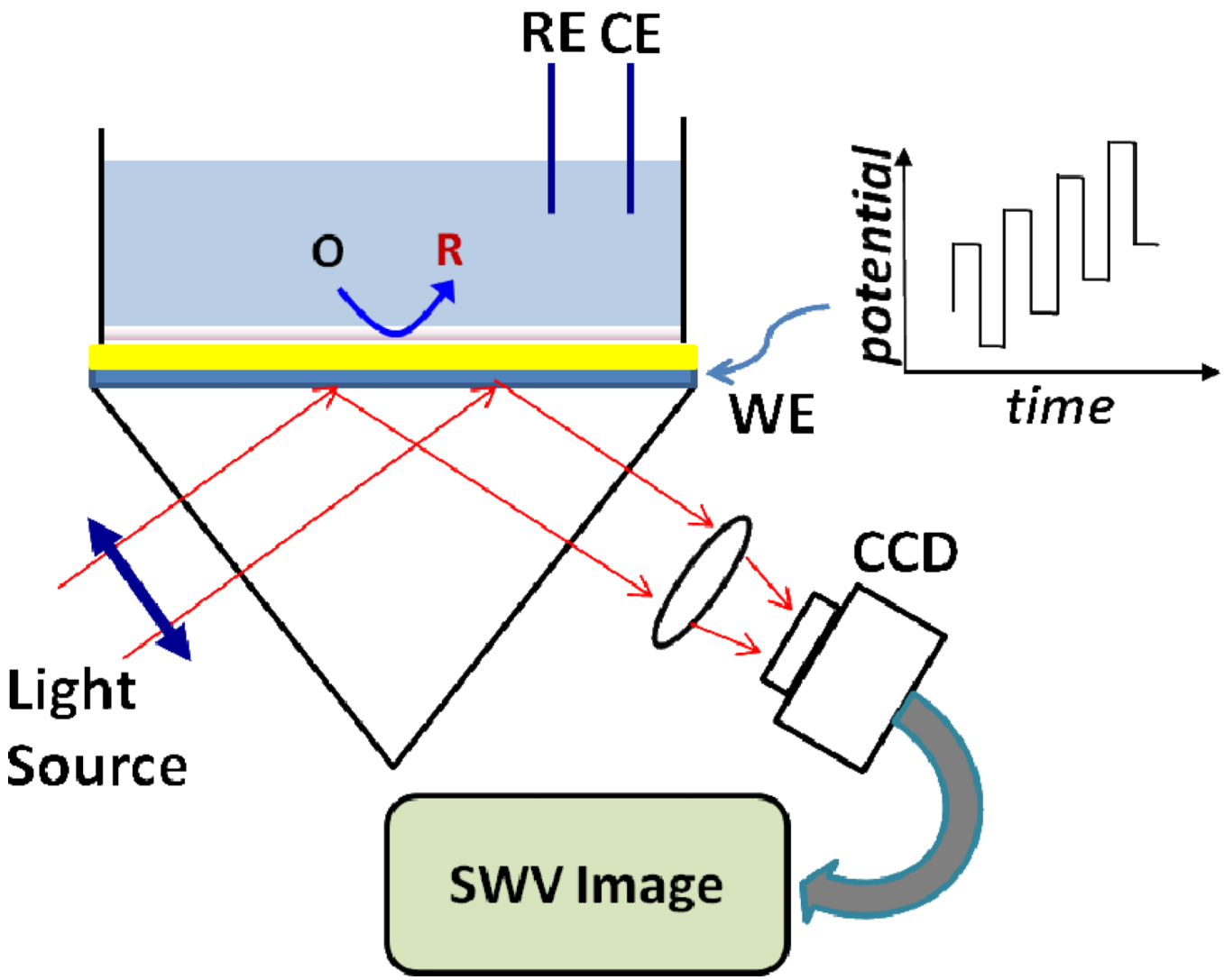

Scheme 1.
Experiment setup of SWV imaging. See text for details.